Endocranial Morphology of *Microchoerus erinaceus* (Euprimates, Tarsiiformes) and Early Evolution of the Euprimates Brain

Anusha Ramdarshan and Maeva J. Orliac*

Paleontology division, Institut des Sciences de l'Evolution, UMR 5554 CNRS, IRD, EPHE, Université De Montpellier, 34095 Montpellier Cedex 5, France

KEY WORDS primate; endocast; Late Eocene; CT scan; Omomyiformes

ABSTRACT

Objectives: Innovations in brain structure and increase in brain size relative to body mass are key features of Primates evolutionary history. Surprisingly, the endocranial morphology of early Euprimates is still rather poorly known, and our understanding of early euprimate brain evolution (Eocene epoch) relies on a handful of specimens.

Materials and Methods: In this article, we describe the endocranial cast of the tarsiiform *Microchoerus erinaceus* from the late Early Eocene of Perrière (Quercy fissure filling, France) based on a virtual reconstruction extracted from CT scan data of the endocranial cavity of the complete, undeformed specimen UM-PRR1771.

Results: The endocast of *M. erinaceus* shows the derived features observed in other Euprimates (e.g. sylvian fissure and temporal lobe), with limited neocortical folding, and a telencephalic flexure comparable to that of extant primates.

Discussion: Comparison with the endocasts of other available late Eocene primates shows that they already exhibited a variety of brain morphologies, highlighting the complex history of the external features of the primate brain, as early as the Eocene. *M. erinaceus* was a fruit and gum eater considered as nocturnal based on its orbit size. However, its brain showed small olfactory bulbs—smaller than in the coeval diurnal taxa *Adapis parisiensis*—and a neocorticalization similar to folivorous taxa. These observations contrast with patterns observed in primates today where nocturnal taxa have larger olfactory bulbs than diurnal taxa, and call into question a direct correlation between frugivory and neocorticalization increase in primates. Am J Phys Anthropol 159:5–16, 2016.

Innovations in brain structure and increase in brain size relative to body mass are key features of Primates evolutionary history. Crown-clade primates or Euprimates, are documented in the fossil record back to the late Paleocene (*Altiatlasius*; Sigé et al., 1990). Documented endocranial casts of early Euprimates show that they already present a derived morphology of the brain with the presence of the sylvian complex, a prominent structure of the brain which divides the frontal lobe from the temporal lobe, with the exception of *Smilodectes gracilis* (Gazin 1965: plate1). They also already show a larger brain size relative to their body mass than the average of mammals of the same time (Bloch and Silcox, 2006; Silcox et al., 2009). As such, recent studies on the evolutionary history of the primate brain mainly focused on euprimates relatives, the Plesiadapiformes, in order to decipher the initial phase of their brain differentiation (Silcox et al., 2009; Silcox et al., 2010; Orliac et al., 2014).

However, surprisingly, the endocranial morphology of early Euprimates is still rather poorly known. Endocranial casts of Adapiformes are mainly documented in the literature by two taxa only, each represented by a unique specimen, *Adapis parisiensis* (Gingerich and Martin, 1985), and *Smilodectes gracilis* (Gazin, 1965). Two partial endocasts documenting the anterior-most part of the brain are also available for *Notharthus* (Gurche, 1982: Fig. 5), and endocranial data (cranial capacity) is available for *Pronycticebus gaudryi* (Martin, 1990) but no specimen is depicted. For Tarsiiformes (comprising paraphyletic Omomyiformes plus Tarsiidae, according to the results of Ni et al., 2013: Fig. 1) partial descriptions of the endocasts of *Necrolemur antiquus* (Microchoeridae; Hürzeler, 1948) and *Tetonius homunculus* (Omomyinae; Radinsky, 1967) are available based on natural endocranial casts. More

Additional Supporting Information may be found in the online version of this article.

Abbreviations: al, alisphenoid; bs, brainstem; bvc, blood vessel canal; cev, capsuloparietal emissary vein canal; cf, circular fissure; eam, external auditory meatus; gs, glenoid surface; ips, inferior petrosal sinus; llc, lateral lobe of cerebellum; lsl, lateral sulcus; nc, neocortex; ob, olfactory bulb; on, optic nerve; otc, orbitotemporal canal; pc, paleocortex; pf, paraflocculus; pgvc, postglenoid vein canal; pi, pituitary; pmf, paramedian fissure; pt, pterygoid; sf, sylvian fossa; ss, sagittal sinus; tb, tympanic bulla; ts, transverse sinus; tsl, temporal sulcus; vm, vermis

Anusha Ramdarshan and Maeva J. Orliac contributed equally to the publication.

*Correspondence to: Maeva Orliac, Institut des Sciences de l'Evolution, UMR 5554 CNRS, IRD, EPHE, CC064, Université de Montpellier, Place Eugène Bataillon, 34095 Montpellier Cedex 5, France. E-mail: maeva.orliac@univ-montp2.fr

Received 17 March 2015; revised 31 August 2015; accepted 2 September 2015

DOI: 10.1002/ajpa.22868

Published online 21 September 2015 in Wiley Online Library (wileyonlinelibrary.com).

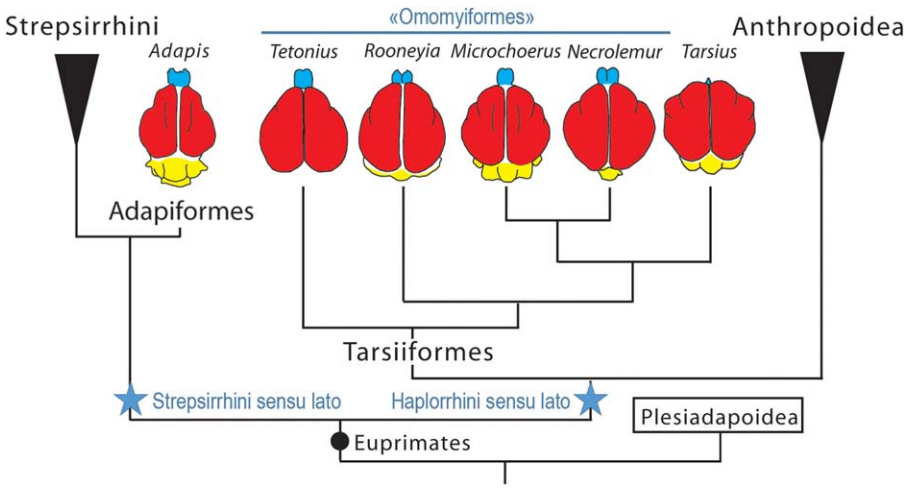

Fig. 1. Endocast morphology and relationships for Euprimates. Topology based on a simplified version of the Figure 3 of Ni et al. (2013); relationships between Euprimates and Plesiadapoidea from Bloch et al. (2007).

recently, the advent of new imagery techniques based on computed tomography has allowed access to a new source of data. Based on CT-scan investigation, Kirk et al. (2014) described the endocranial morphology of the Late Eocene taxon *Rooneyia viejaensis*, another Tarsiiformes taxa (for alternative phylogenetic position of *Rooneyia* see Szalay, 1976; Rosenberger, 2006; Rosenberger et al., 2008). To sum up, our understanding of early euprimate brain evolution (Eocene period) only relies on a handful of specimens, two of which are documented only by summary descriptions.

Here, we describe the endocranial morphology of an exceptionally well preserved cranium of the microchoerid *Microchoerus erinaceus* (UM-PRR1771) from the Late Eocene locality of Perrière (MP 17b, ca. 37 Ma, Biochrom'97), a fissure filling from the Quercy region in the South of France. The specimen UM-PRR1771 has previously only been used in a microwear study (Ramdarshan et al., 2012), and its cranial morphology remains undescribed. *M. erinaceus* has been recorded in European localities ranging from the late Middle to Late Eocene (Ramdarshan et al., 2012). Microchoeridae are small- to medium-sized European non-anthropoid haplorhines, closely related to the extant *Tarsius* (Fig. 1). The endocast of *M. erinaceus* further documents the external morphology of the brain of Eocene Euprimates in general and microchoerids in particular (so far only partially known by *Necrolemur antiquus*, Hürzeler, 1948).

MATERIAL AND METHODS

Material

The specimen UM-PRR1771 described here consists of an almost complete undeformed cranium, lacking only the postorbital bar on the left side, and part of the temporal and petrosal bones on the right side. The specimen is curated at the Université de Montpellier, France. UM-PRR1771 was scanned with the Scanco UCT80 at the Anthopological Institut and Museum, Zürich. The voxel size is 0.05 mm. The three-dimensional (3D) segmentation of bone, endocast, and sinuses was performed using the segmentation threshold selection tool of AVIZO 7.1 (Visualization Sciences Group). The cranial bone, endocast, and sinuses were selected in separate labelfields, to which different colors and transparencies were applied. The labeled 3D model of the endocast and sinus of UM-PRR1771 is available at MorphoMuseuM.com, model ID: M3#15_UM-PRR1771. Measurements were taken using calipers on the actual specimen (orbit diameter, cranium length) or with AVIZO 7.1 (endocast). Total endocast volume has been calculated by surface integration using the same software. Subvolume of the olfactory bulbs and surface areas were calculated using ISE-MeshTool (Lebrun, 2014).

Methods

Body mass estimates, encephalization quotients, and neocorticalization ratio. Body mass estimates were calculated from different proxies, using the regression of (i) the area of the first lower molar (Conroy, 1987), (ii) area of the first upper molar (Gingerich et al., 1982), (iii) cranial length (generic primate equation of Martin, 1990), and postcranial measurements (talus dimensions, Dagosto and Terranova, 1992). Body mass estimate confidence intervals were calculated and boxplots were drawn using R (R Core Team, 2015). The encephalization quotients (EQ) were calculated using different body mass estimates values and different equations: (i) Jerison (1973), (ii) Eisenberg (1981), (iii) Martin (1990). The neocorticalization ratio is measured as the surface area of neocortex relative to the entire endocast surface area reduced by olfactory bulbs (Jerison, 2012: 386): Neocorticalization ratio = total neocortex surface area/(total surface area – olfactory bulbs surface area). Surface of the neocortex selected to calculate the neocorticalization ratio of *Microchoerus erinaceus* and *Rooneyia viejaensis* is illustrated in Supporting Information Figure 1a.

Optic foramen index and quotient. Measurements of the optic foramen are relevant to assessing activity period in living primates (Kay and Kirk, 2000; Kirk and Kay, 2004), and measurement of the size of the optic foramen gives an idea of the activity pattern of extinct forms. The optic foramen index was calculated following Kay and Kirk (2000) using the following equation: $OFI = 100 \times (\text{optic foramen area}/\text{orbit diameter}^2)$. The

optic foramen quotient was calculated following Kirk and Kay (2004) using the equation: [OFQ = 100 × (observed OFI-expected OFI/expected OFI).

Basicranial flexion. Ross and Ravosa (1993) define basicranial flexion as follows: "pre- and post-sella portions of the cranial base are downwardly or ventrally deflected relative to each other so that the endocranial and/or exocranial surfaces of those bones do not lie in a single plane, but form a ventrally open angle of less than 180° with each other" (Ross and Ravosa, 1993: 305). Most studies on basicranial flexion in primates rely on craniometric landmarks and angular measurements based on bones of the braincase (e.g. Ross and Ravosa, 1993; Straight, 1999; McCarthy, 2001; Ross et al., 2004). Basicranial flexion is directly correlated to the flexion observed on endocranial casts, also described as telencephalic flexure (Dechaseaux, 1962). We measured the cranial base angle (CBA) of *M. erinaceus*, on the sagittal plane of the skull following the protocol of Ross and Ravosa (1993: Fig. 2). The CBA corresponds here to the angle between the plane of the ventral border of the medulla (plane of clivus ossis occipitalis) and the plane corresponding to the planum sphenoideum (see Supporting Information Fig. 2 for graphic reconstruction).

RESULTS

Description and comparisons

The braincase of *M. erinaceus* occupies most of the volume of the cranium, and extends more than half of the total length of the skull (Fig. 2). The gross morphology of the endocast of *M. erinaceus* resembles that of *R. viejaensis* or *A. parisiensis*, and shows the derived features observed in Euprimates: demarcation of the temporal lobe, lack of exposure of the midbrain, a posterior location of the optic chiasma (closer to pituitary compared with plesiadapiforms), and presence of a sylvian fissure (Orliac et al., 2014). The total volume of the virtual endocast is 4.26 cm^3 (Table 1).

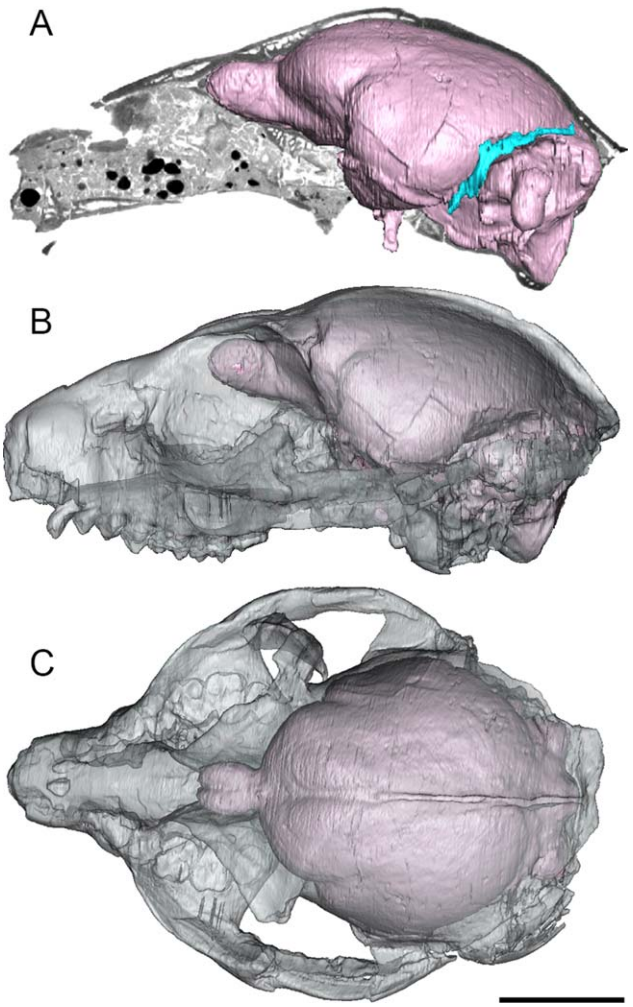

Fig. 2. In situ three-dimensional reconstructions of the endocast of *Microchoerus erinaceus* (UM-PRR 1771). **A**) Parasagittal slice showing in situ three-dimensional reconstructions of endocranial structures near the midsagittal plane. **B** and **C**) endocast viewed through a translucent rendering of the cranium in B) left lateral, and (C) dorsal views. Scale bar, 1 cm.

Rhinencephalon. The anterior-most part of the olfactory bulbs extends between the two orbits, anterior to the post-orbital bar and reaches as far as the first third of the orbit (Fig. 2). The olfactory bulbs are small relative to the cerebrum width, joined for most of their length and separated from the cerebral hemispheres by a shallow circular fissure (Fig. 3C), a primitive condition for Euprimates (Orliac et al., 2014). A circular fissure can be seen in Plesiadapiformes such as *Plesiadapis* (Gingerich and Gunnell, 2005; Orliac et al., 2014), *Ignacius* (Silcox et al., 2009), or *Microsyops* (Silcox et al., 2010). It is also present but reduced in the Eocene adapiform *A. parisiensis* (Radinsky, 1970), but not in the tarsiiform *R. viejaensis* (Kirk et al., 2014). Concurrently, the neocortex does not completely cover the olfactory peduncles in *M. erinaceus*. The olfactory bulbs represent 0.96% of the overall braincase volume (Table 1). This is approximately the same as in *R. viejaensis* (0.94%) and *N. antiquus* (0.87%) but far less than in *A. parisiensis* (3.03%) or *T. homunculus* (3.40%).

Cerebrum. The neocortex extends well above both the olfactory bulb and orbit levels (Fig. 2A,B). The part of the cerebrum anterior to the sylvian fissure shows a wide depression for the orbit fossa. The neocortex surface bears three sulci of different depths: a deep sylvian fissure, a shallow lateral sulcus, and a faint sulcus on the temporal lobe, posterior to the sylvian fissure. This faint inflexion of the surface of the temporal lobe, by its location is called the temporal sulcus. Such a structure is neither present in *R. viejaensis* nor in *A. parisiensis* (Fig. 4), and is not represented in *T. homunculus* and *N. antiquus* according to Radinsky's (1970) drawings. Noteworthy, it can be seen in extant strepsirhines like *Perodicticus potto* or *Galago senegalensis* (Radinsky, 1968).

On the dorsal surface of the cerebral hemispheres, the shallow lateral sulcus is parallel to the superior sagittal sinus. It is mostly marked on the middle of the cerebrum, but extends anterior to the level of the sylvian fissure. The sylvian fissure deeply indents the neocortex and delimitates a wide temporal lobe. The latter extends ventral to the orbitotemporal canal and its ventral

TABLE 1. Endocast measurements for M. erinaceus *and other Eocene Euprimates*[a]

	Microchoerus erinaceus	Rooneyia viejaensis	Adapis parisiensis	Necrolemur antiquus	Tetonius homonculus
Volume (cm^3)	4.26	7.23	8.8	3.8	1.5
Total endocast surface area (mm^2)	1,866.67	2,409.33	–	–	–
Neocortex surface area (mm^2)	771.76	1,054.55	–	–	–
Neocotical ratio	0.41	0.44	0.43–0.53	0.56	–
Total endocast length (mm)	31.44	628.03	–	–	–
Cerebrum maximal length (mm)	22.53	513.01	–	–	–
Cerebrum maximal width (mm)	23.12	449	–	–	–
Olfactory bulbs length (mm)	4.51	71.04	–	–	–
Olfactory bulbs maximum width (mm)	4.46	105	–	–	–
Volume of olfactory bulb (cm^3)	0.041	0.068	0.267	0.033	0.051
PVOB (%)	0.96	0.94	3.03	0.87	3.4
Telencephalic flexure (CBA)	161°	176°	187°	165°	–
OFI	1.35	1.76	0.78	1.34	–
OFQ	−53	−37.34	−66.62	−59.72	–

[a] The optic foramen index [OFI = 100 × (optic foramen area/orbit diameter^2) is calculated following Kay and Kirk (2000). The optic foramen quotient [OFQ = 100 × (observed OFI-expected OFI/expected OFI) is calculated following Kirk and Kay (2004). PVOB corresponds to the percentage of endocast volume occupied by olfactory bulbs. OFI and OFQ for *R. viejaensis, A. parisiensis* and *N. antiquus* after Kay and Kirk (2000). Endocast volume of *A. parisiensis*, *N. antiquus*, and *T. homonculus* after Gingerich and Martin (1981), Radinsky (1977), and Long et al. (2015), respectively. Neocortical ratios of *A. parisiensis* and *N. antiquus* after Long et al. (2015).

extremity is rounded and points ventrally. In *R. viejaensis*, the ventral extension of the temporal lobe below the orbitotemporal canal is more important (implying more paleocortex), and its ventral extremity points more anteriorly. The rhinal fissure is not visible on the specimen UM-PRR1771. The orbitotemporal canal, well-marked on the *M. erinaceus* endocast, is considered a good approximation of the location of the rhinal fissure in primates based on observations in extant lemurs (Radinsky, 1974), and therefore, would mark the limit between neocortex and palaeocortex. The location of the orbitotemporal canal is roughly the same in *R. viejaensis* and in *M. erinaceus*. In *A. parisiensis*, the orbitotemporal canal is also very low down on the endocast (Radinsky, 1970; Gingerich and Martin, 1981); but the size of the temporal lobe is small compared with *R. viejaensis* and *M. erinaceus* (Fig. 4D vs. Fig. 4F,H). In *A. parisiensis*, in lateral view, the rhinal fissure is located at half of the height of the sylvian fissure and cuts the temporal lobe into two sub-equal areas, whereas in *R. viejaensis* and *M. erinaceus* a greater surface of the temporal lobe lies above the level of the rhinal fissure. This would imply proportionally more neocortex and less paleocortex in the temporal lobe of *A. parisiensis*. The orbitotemporal canal is neither visible in *T. homunculus* (Radinsky's drawings 1968), nor in *N. antiquus* (Hürzeler, 1948). As described in *R. viejaensis* (Kirk et al., 2014), the virtual endocast of *M. erinaceus* also lacks a well-developed impression for the petrosquamous sinus caudal to the postglenoid foramen. As in *R. viejaensis*, this petrosquamous sinus is fully enclosed in a bony canal ("temporal canal" of Diamond, 1992) for most of its length (Fig. 3A). By contrast, in *Tarsius*, (like in *Microcebus* and *Loris* endocasts Kirk et al., 2014, Fig. 4), most of the course of the petrosquamous sinus leaves an impression on the caudal surface of the endocast's temporal region.

The posteriormost part of the cerebrum is only slightly domed. It extends onto the midbrain and covers part of the cerebellum beyond the part directly above the basis of the parafloccular lobes (Fig. 3C,E). This is similar to *R. viejaensis* but differs from *A. parisiensis* in which the posterior extension of the neocortex is less pronounced (Fig. 4E vs. 4G,I). There is a deep notch on the postero-ventral border of the hemisphere. This depression is occupied by the very large petrosal bone; more precisely by the hyperinflated pars mastoidea housing the depression of the subarcuate fossa (enclosing the strongly projecting flocculo-paraflocular lobe) and by the anteriorly protruding tympanic bulla.

Cerebellum. As mentioned above, a large portion of the cerebellum is covered by the cerebrum. Both are separated by a salient transverse sinus. The cerebellum of *M. erinaceus* consists in three portions of equal size: the vermis and the two lateral lobes (cerebellar hemispheres). The paraflocculi are large; they protrude laterally and ventrally and are widely visible in dorsal view (i.e. not completely covered by the posterior extension of the neocortex). The paraflocculi are elongated ventrally and oval in shape compared with *R. viejaensis* and *Tarsius* (*T. syrichta*, Stephan, 1984), and to extant strepsirhines (*Microcebus rufus*, *Loris tardigradus*; Kirk et al., 2014) where it is more spherical. This structure is broken away on the *A. parisiensis'* endocast (Gingerich and Martin, 1981) and is neither preserved on *N. antiquus* nor *T. homunculus*. Two paramedian fissures separate the vermis from the lateral lobes of the cerebellum in *M. erinaceus*. The vermis itself is subdivided by three fissures of similar depth, and the fissura prima cannot be distinguished from the other cerebellar fissures. Most of the lateral side of the cerebellum is in contact with the petrosal bone which confers a singular shape to the lateral lobes, with two parts protruding dorsally.

Encephalization quotient and neocorticalization ratio. The encephalization quotient (EQ) corresponds to brain size expressed as a function of body mass (Jerison, 1973). Body mass of *M. erinaceus* is estimated at 597g (95% confidence limits: 430 to 763 g; Ramdarshan et al., 2012) based on the length of the first lower molar (Conroy, 1987). Other proxies of body mass estimates i.e., first upper molar surface (Conroy, 1987), cranial length (Martin, 1990), and postcranial measurement (talus dimensions, Dagosto and Terranova, 1992) provide

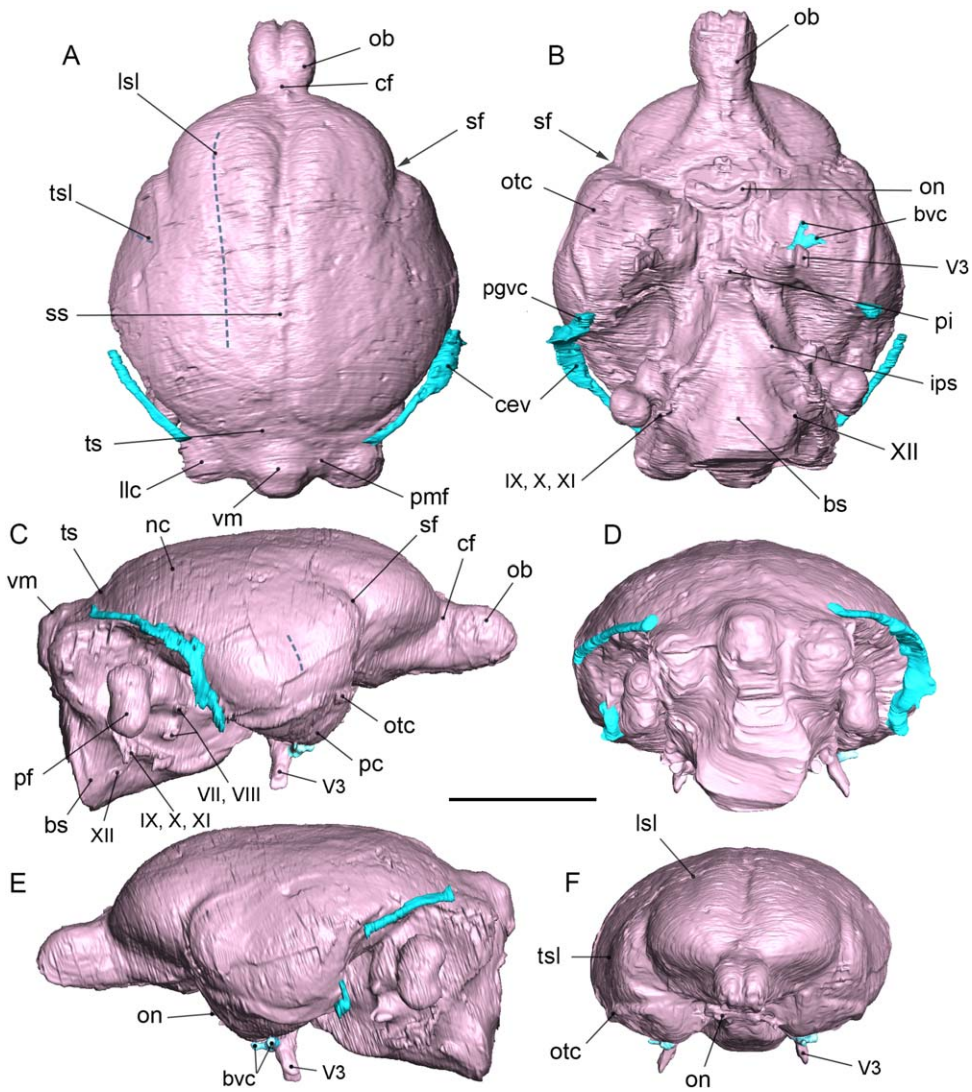

Fig. 3. Labeled endocast and sinus of *Microchoerus erinaceus* (UM-PRR 1771) in **A**) dorsal **B**) ventral, **C**) right lateral, **D**) posterior, **E**) left lateral, and **F**) anterior views. Dotted lines underline cortical sulci. Numbers IV–XII refer to cranial nerves; V1–V3 refer to different branches of nerve V. Scale bar, 1 cm.

results for *M. erinaceus* ranging between 241 g and 642 g (Table 2). The EQs calculated using these different body mass values ranges from 0.49 to 1.07 depending on the equation used [Jerisons (1973) equation, Eisenbergs (1981) equation, or Martins (1990), Table 2].

In *M. erinaceus*, the total surface area of the endocast equals 1866.7 mm^2, the olfactory bulbs surface equals 71.0 mm^2 and the neocortical surface equals 771.6 mm^2, which corresponds to a neocorticalization ratio of 41.3% (Table 1). This ratio was calculated for *R. viejaensis* based on the 3D model provided by Kirk et al. (2014; for neocortex surface area see Supporting Information Fig. 1a) and a slightly superior value was obtained (neocorticalization ratio of *R. viejaensis* = 43.8%).

Cranial nerves and identification of basicranium and orbitosphenoid foramina. Micro-CT images of UM-PRR 1771, together with direct observation of the basicranium and orbit region have facilitated proposing hypotheses of identification of cranial nerves and sinuses. The orbits, partially filled with sediments in the specimen, were virtually cleaned in order to identify the location of the optic foramen and surrounding features. The bone of the braincase is very thin and partially broken, but combining left and right sides allows reconstructing the complete pattern of foramina of the alisphenoid/orbitosphenoid region (Fig. 5). On the ventral surface of the endocast, casts of the optic chiasma are preserved and are situated at the level of the anterior edge of the pyriform lobes. The optic foramen can accordingly be located as illustrated in Figure 5. The optic foramen is large (surface area = 2.43 mm^2) and represents the medial most foramen of the orbit. There is no trace of an ethmoid foramen on the virtual specimen contrary to the microchoerid *N. antiquus* (Simons and Russell, 1960). Lateral and posterior to the optic foramen, on the parietal bone is a small foramen, also figured in *Necrolemur* (Simons and Russell, 1960, Fig. 3), which corresponds to the cranio-orbital foramen that

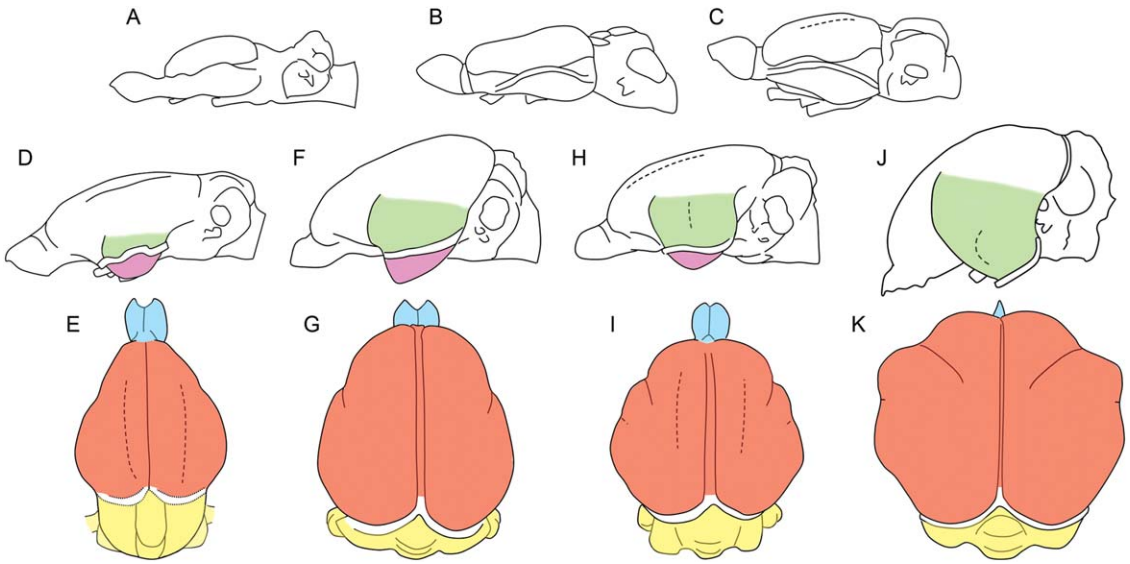

Fig. 4. Schematic views of the external features of some primates endocasts. **A**) *Plesiadapis tricuspidens* (after Orliac et al., 2014); **B**) *Ignacius graybullianus* (after Silcox et al., 2009); **C**) *Microsyops annectens* (Silcox et al., 2010); **D** and **E**) *Adapis parisiensis* (Cambrigde skull, M538); E and **F**) *Rooneyia viejaensis* (alter Kirk et al., 2014); **G**, **H**) *Microchoerus erinaceus* (UM-PRR 1771); *I*, *J*) *Tarsius* (after Radinsky, 1968). A–C, D, F, H, J dorsal views; E, G, I, K, lateral views. Colors: pink, pyriform lobe; green, neocortical part of the temporal lobe (roughly delimited between dorsal end of sylvian fissure and maximal concavity of the posterior edge of neocortex); blue, olfactory bulbs; red, cerebrum; yellow, cerebellum. Not to scale.

TABLE 2. Body mass estimations (in g) according to different proxies and corresponding encephalization quotients according to different equations[a]

	Microchoerus erinaceus	Rooneyia viejaensis	Adapis parisiensis	Necrolemur antiquus	Tetonius homonculus
EV (cm^3)	4.26	7.23	8.80	3.80	1.50
BM (m1)[b]	597 (463–1370)	–	2350 (1778–2566)	233 (177–674)	74 (50–171)
EQ 1	0.49 (0.28–0.58)	–	0.4 (0.38–0.49)	0.82 (0.40–0.99)	0.69 (0.40–0.91)
EQ 2	0.68 (0.37–0.82)	–	0.51 (0.48–0.63)	1.22 (0.56–1.50)	1.13 (0.61–1.51)
EQ 3	0.56 (0.30–0.68)	–	0.41 (0.38–0.51)	1.02 (0.46–1.26)	0.97 (0.51–1.30)
BM (M1)[b]	1150	1014	1911	452	295
EQ 1	0.32	0.58	0.46	0.53	0.28
EQ 2	0.42	0.78	0.60	0.75	0.41
EQ 3	0.34	0.64	0.48	0.62	0.34
BM (CL)	241	381	1863	178	–
EQ 1	0.90	1.12	0.47	0.98	–
EQ 2	1.34	1.62	0.61	1.49	–
EQ 3	1.12	1.34	0.49	1.26	–
BM (PC)[c]	642 (345–1508)	–	1544 (776–2763)	194 (64–465)	113 (28–277)
EQ 1	0.47 (0.27–0.71)	–	0.53 (0.36–0.85)	0.93 (0.52–1.95)	0.53 (0.29–1.34)
EQ 2	0.65 (0.35–1.04)	–	0.70 (0.45–1.16)	1.40 (0.73–3.18)	0.82 (0.42–2.32)
EQ 3	0.53 (0.28–0.86)	–	0.56 (0.70–1.18)	1.18 (0.61–2.74)	0.70 (0.35–2.02)

Confidence intervals provided in brackets.
[a] Body mass estimations (BM) from this study calculated using the following equations: BM (m1), using the length of the lower m1 (Conroy, 1987); BM (M1), using upper M1 surface (Gingerich, 1982); BM (CL), using cranial length (generic primate equation of Martin, 1990); BM (PC), using talus measurements (Dagosto and Terranova, 1992). Encephalization quotient (EQ) using the equations of Jerison (1973, EQ1), Eisenberg (1981, EQ2), and Martin (1990, EQ3). First lower molar dimensions used are from Ramdarshan et al. (2012) and Ramdarshan et al. (2011). First upper molar dimensions used are from this study, Ramdarshan et al. (2011), and Szalay (1976). Cranial length values used are from this study and from Kirk et al. (2014). The postcranial body mass estimates used in this study are the mean of the estimates published in Dagosto and Terranova (1992).
[b] Body mass estimates and confidence intervals from Ramdarshan et al. (2011).
[c] Body mass estimates and confidence intervals from Dagosto and Terranova (1992).

is the anterior opening of the orbitotemporal canal that typically transmits the ramus superior of the stapedial artery and the accompanying cranio-orbital venous sinus (Diamond, 1992). Just ventrolateral to the optic foramen lies a slightly smaller foramen referred to as the fusion of the foramen rotundum and anterior lacerate foramen by Simons and Russell (1960) in *N. antiquus*. Identification of this foramen therefore directly relies on the absence of an individualized foramen rotundum. Our reconstruction shows that the foramen ovale opens on the external side of the external pterygoid wall and communicates laterally with two other little foramina, which

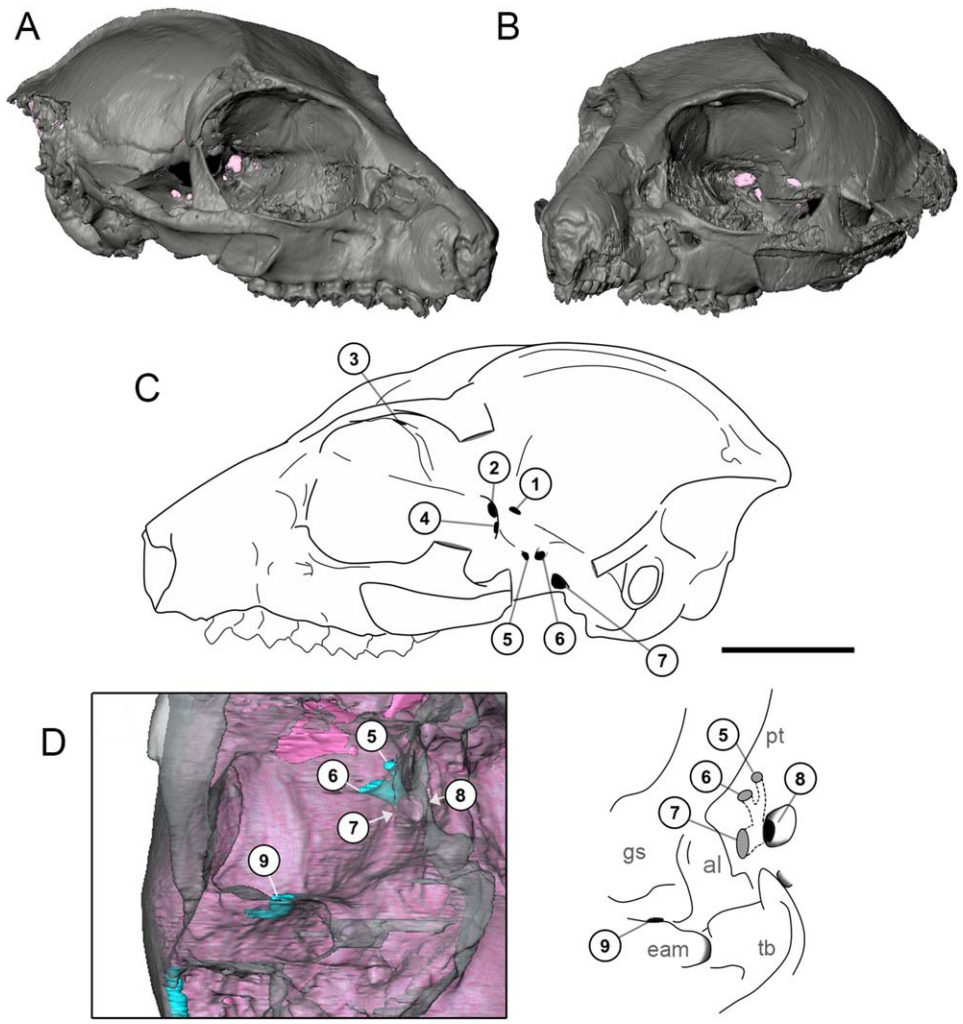

Fig. 5. Identification of orbitosphenoid foramina of *Microchoerus erinaceus* (UM-PRR 1771), after in situ reconstruction of pathways of cranial nerves (red) and blood vessels (blue), **A** and **B** show right and left views of the virtually cleaned orbits of UM-PRR 1771 showing the foramina labelled in the composite view **C**. Proposed identification of foramina: 1, cranio-orbital foramen; 2, optic foramen; 3, supraorbital foramen; 4, foramen rotundum + sphenorbital fissure; 5 to 6, blood vessel pathway (internal pterygoid branch of the internal maxillary artery); 7, foramen ovale; 8, alisphenoid canal; 9, foramen postglenoid. Scale bar, 1 cm.

results in a trifurcation, at the level of cranial nerve V. These three branches could represent the branches V1, V2, and V3 of the trigeminal nerve. Accordingly, the foramen directly anterodorsal to the foramen ovale would correspond to the foramen rotundum, pathway of the branch V2. This interpretation would be consistent with that of Gregory (1915) for the similar structure in *Necrolemur*. However, this small foramen opens on a groove on the external surface of the alisphenoid bone, oriented dorsally and slightly backward. The maxillary branch of the trigeminal nerve innervates a rather anterior portion of the head, e.g. the cheeks and maxillary region, and the nose region. This nerve is therefore expected to exit towards the anterior of the head, as opposed to posterodorsally. On *Necrolemur*, Simons and Russell (1960) interpreted the small foramina anterior to the foramen ovale on the external surface of the alisphenoid as the pathway for the internal pterygoid branch of the internal maxillary artery. In *Necrolemur*, a large and well-delimited foramen opens on the internal side of the alisphenoid pterygoidal wing, which was identified as the alisphenoid canal by Simons and Russell (1960), whereas Szalay (1976: Fig. 12) identified it as the foramen ovale. A similar foramen is found in the basal gliroid *Rhombomylus* and referred to as the medial foramen ovale by Meng et al. (2003). Observation of CT scan slices of UM-PRR 1771 show that a similar large foramen communicates laterally with the foramen ovale posteriorly and with the two other smaller foramina anteriorly (Fig. 5D). We interpret the two foramina anterior to the foramen ovale in *M. erinaceus* as foramina for blood vessel supply. Given these interpretations of the foramina of the alisphenoid region, the foramen apposed to the optic foramen is interpreted as the confluence of the foramen rotundum with the sphenorbital fissure (also referred as "foramen orbitorotundum," NAV).

The postglenoid foramen, pathway of the postglenoid vein, is located posterolaterally to the foramen ovale, posterior to the glenoid surface. Casts of the cranial nerves VII and VIII can be seen on the endocast, located just ventrally to the paraflocculus (Fig. 3B,C,E). The jugular foramen can be clearly seen between the bulla and the

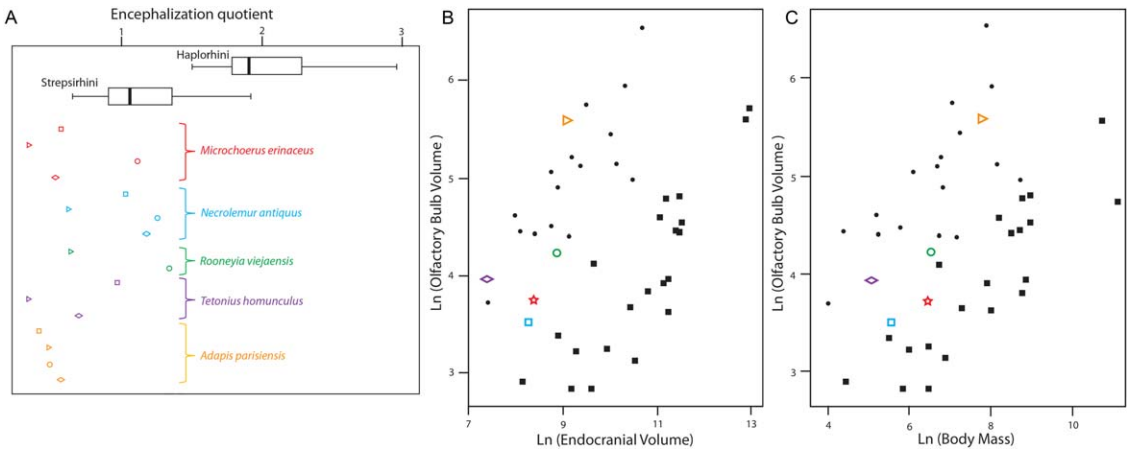

Fig. 6. **A**) Encephalization quotients of paleogene Euprimates discussed in this study compared to extant primates estimated according to Martin (1990). Mean EQs for fossil taxa were estimated using different body mass estimations: lower m1 area (square), upper M1 area (triangle), cranial length (circle), and postcranial measurements (diamond). See Table 2 for corresponding references. **B** and **C**) Bivariate plots of ln olfactory bulb volume vs. (B) ln endocranial volume, and (C) ln body mass for paleogene Euprimates discussed in this study and extant primates; empty star, *M. erinaceus*; empty triangle, *A. parisiensis*; empty diamond, *T. homunculus*; empty circle, *R. viejaensis*; empty square, *N. antiquus*; black points, extant Strepsirhines; black squares, extant Haplorhines. The mean values of body mass estimates has been considered in (C). Comparative data from Silcox et al. (2009).

condyle. It flanks the posteromedial side of the bulla. Immediately anterior to the jugular foramen, the foramen caroticum, which would have housed the carotid artery is also visible. In *Necrolemur*, an additional foramen ["foramen of unknown meaning" of Hurzeler (1948: Fig. 28)] is present immediately next to the foramen caroticum. In *R. viejaensis*, this foramen is also present and is identified as the internal petrous sinus (Szalay, 1976). No evidence for this foramen can be seen in *M. erinaceus*. The cast of the hypoglossal foramen (cranial nerve XII) is visible on the brainstem, posteromedial to the jugular foramen.

Optic foramen index and optic foramen quotient. The orbit diameter of *M. erinaceus* (UM-PRR1771) measures 13.38 mm for a skull length of 49.8 mm; the cross-sectional area of the optic foramen equals 2.43 mm^2. The optic foramen index (OFI) equals 1.35 in *M. erinaceus* and the optic foramen quotient (OFQ) equals −53.00 (OFI expected = 2.89). Both values calculated for *M. erinaceus* are slightly higher than those proposed by Kay and Kirk (2004) for *Microchoerus* sp. (MNHN QU 10879; OFI = 1.29; OFQ = −58.82).

Telencephalic flexure. The CBA of *M. erinaceus* equals 161° (for corresponding slice see Supporting Information Fig. 2). A similar result (162°) is obtained measuring the corresponding angle on the endocast, using the outlines of the cross-section at the sagittal plane (see Supporting Information Fig. 2). CBA values of extant primates roughly range between 190° and 140°. The CBA value of *M. erinaceus* is similar to that of extant primates such as *Loris tardigradus* (Lorisidae, Strepsirhini), *Cebuella pygmaea* (Callitrichidae, Haplorhini), or *Hylobates muelleri* (Hominoidea, Haplorhini) (Ross and Ravosa, 1993: Table 1). The value calculated for *M. erinaceus* is very close to that measured for *N. antiquus* (165°, maphq289). Both clearly differ from that of *A. parisiensis* for which the CBA exceeds 180° (187°, Cambridge specimen M538, Table 1, Supporting Information Fig. 2). The telencephalic flexure of *R. viejaensis*, estimated from the 3D model of its endocasts provided by Kirk et al. (2014), equals 176°.

DISCUSSION

According to recent hypotheses (Ni et al., 2013), the extant Tarsiidae *Tarsius* would be nested within paraphyletic Omomyiformes and form with them theTarsiiformes clade (Fig. 1). Anthropoidea would then be sister group to Tarsiiformes, making up the Haplorhinni sensu lato (versus Haplorhinni sensu stricto corresponding to the grouping of extant primates with postorbital closure only i.e. *Tarsius* + Anthropoidea). This wide Haplorhinni group is sister taxa to Strepsirhini sensu stricto, the living "tooth-combed" primates and its sister clade, the extinct Adapiformes, "lemur-like" primates of the Eocene epoch, which were non tooth-combed. Endocasts of extinct Euprimates provide us with precious data about the external morphology of the brain of Late Eocene taxa related to Haplorhinni and to Strepsirhini clades and allow discussing the evolutionary stage of their brain evolution.

Encephalization and neocorticalization of *M. erinaceus* among early euprimates

Comparisons of the EQ of *M. erinaceus* calculated using different body mass values with the corresponding values for some other Eocene Euprimates is presented in Table 2. EQ values vary greatly depending of the body mass estimation proxy used, which makes it difficult to properly compare EQ values of extinct Euprimates. Due to differences in dental, cranial and postcranial morphology of the taxa compared here, relative EQs of taxa differ depending on body mass estimates proxies (Table 2, Fig. 6A). On the other hand, encephalization quotients are inherently dependant on body mass estimates, for which error rates are significant (up to 30%) and confidence intervals are large (e.g., Conroy, 1987; Dagosto and Terranova, 1992; Ford and Davis, 1992; Smith,

2002; LaBarbera, 2007). In this context, differences in EQ may not be significant, and interpretations of these differences need to remain tentative. Keeping all these problems in mind, generally speaking, *N. antiquus* and *R. viejaensis* have the highest EQ values as illustrated on Figure 6. If we consider the mean value of available body mass estimates, *N. antiquus* would have the biggest EQ, then *R. viejaensis*, *M. erinaceus*, *T. homunculus*, and *A. parisiensis* would have the smallest EQ. Compared with extant taxa, *M. erinaceus* shows a lower EQ than extant haplorhines, and a significantly lower EQ than *Tarsius*, considered to be the closest extant relative to Omomyiformes [EQ *T. syrichta* = 1.9, using Martins (1990) equation, based on data provided by Silcox et al. (2009)]. The EQ for *M. erinaceus* is indeed more comparable to extant strepsirhines.

The neocorticalization ratios of *M. erinaceus* (41.3%) and *R. viejaensis* (43.8%) are larger to that proposed for the adapiform *S. gracilis* (35.2%, Long et al., 2015), but smaller to that proposed for *A. parisiensis* (51%, Jerison, 2012; 43–53%, Long et al., 2015) and for the microchoerid *N. antiquus* (56.2%, Long et al., 2015). Long et al. (2015) noted that "the more frugivorous fossil Euprimates exhibit the higher neocortical ratios" (Long et al., 2015: 8). Their sample, however, included the neocortical ratio for only one frugivorous/gummivore taxa: *N. antiquus*. According to microwear analysis performed on the material from Perrière, including UM-PRR1771, the diet of *M. erinaceus* was based on fruit and gums (Ramdarshan et al., 2012), just like the coeval microchoerid *N. antiquus*. Based on our results, the frugivorous/gummivore taxa *M. erinaceus* would have a neocorticalization ratio closer to that calculated for folivorous taxa such as *A. parisiensis*, or *Notharctus tenebrosus* (Long et al., 2015), calling into question a direct correlation between frugivory and neocorticalization increase. Neocorticalization could also be impacted by sociality as social factors such as social group size and social complexity could be important to the scaling of the neocortex (e.g., Dunbar and Schultz, 2007). The relatively low neocortical ratio for *M. erinaceus* could reflect the absence of complex social interactions in this taxon.

A general increase in neocortical size through time is observed in mammals (Jerison (2012, Fig. 6). This increase is also observed in Euprimates. Besides, for a given geological age, the neocorticalization ratios of available fossil Euprimates are all superior to the "average" neocorticalization ratio of mammals (Jerison, 2012, Fig. 6; Long et al., 2015: Fig. 4). Modern Euprimates have a neocorticalization ratio greater than 60%, whereas the "average" neocorticalization of mammals is estimated at 51% (Jerison, 2012). The neocorticalization ratio of *M. erinaceus* is consistent with values calculated for other Late Eocene Euprimates (Table 1). As already stated by Jerison (2012) for few fossil Strepsirhines of the Late Eocene, and by Long et al. (2015) for Late Eocene adapids and microchoerids, *M. erinaceus*, part of the Haplorhinni sensu lato, has a neocorticalization ratio smaller than those of extant primates, but larger than the average neocorticalization ratio of mammals at that time (ca. 33%, regression line of Jerison, 2012: Fig. 6). On the other hand, as already stated by Long et al. (2015), the neocorticalization ratios of the available sample of Late Eocene primates, including *M. erinaceus* (i.e. between 0.4 and 0.5) is larger than those estimated for Paleocene and Eocene plesiadapiforms (*Microsyops annectens* = 24.3%; *Ignacius graybullianus* = 21.8–24.4%, Long et al., 2015), including the Euprimateformes *Plesiadapis tricuspidens* (=21.8%, Orliac et al., 2014) of the Late Paleocene, which in turn corresponds to the expected surface area of the brain devoted to neocortex of the average mammals around 55 Ma.

Disposition of brain component and telencephalic flexure of early euprimates

To facilitate comparisons Radinsky (1968) suggested orientating the endocasts with the ventral border of the medulla aligned in the horizontal plane, a recommendation we followed in Figure 4A. Lateral views of the endocranial casts of *A. parisiensis*, *M. erinaceus*, *R. viejaensis*, and *Tarsius* show striking differences in terms of disposition/orientation of the different parts of the brain. The different elements of the brain primitively show a linear organization among Mammalia (Dechaseaux, 1962; Rowe et al., 2011) with the long axis of the olfactory bulbs, cerebrum, cerebellum and the brain stem axis in roughly the same plane in lateral view. The Plesiadapiformes *M. annectens* (Silcox et al., 2010), *I. graybullianus* (Silcox et al., 2009), and *P. tricuspidens* (Orliac et al., 2014) show very weak telencephalic flexure of the brain (Fig. 4A–C).

Among modern Euprimates, *Tarsius* presents one of the more flexed basicrania (Radinsky, 1968; Ross and Ravosa, 1993). This flexion is much less important in Late Eocene tarsiiforms *M. erinaceus* (161°) and *N. antiquus* (165°), however, these two taxa present a higher flexion than their euprimate counterparts, yet the available sample is very reduced (Table 1). Biegert (1963) proposed that basicranial flexion is negatively correlated with the size of the masticatory apparatus. Analysis of the masticatory apparatus in Adapines (Perry, 2002) revealed *Adapis* had well developed jaw adductor muscles; this could be correlated with its small basicranial flexion. *M. erinaceus* and *R. viejaensis* have similar body mass estimates and neocorticalization ratios (Table 2), however, the latter shows a less flexed basicrania. Besides, *R. viejaensis* has a greater EQ, which would have foreshadowed a marked telencephalic flexure (according to the spatial packing hypothesis).

Regardless of the CBA, the orientation of the long axis of the olfactory bulbs of the Late Eocene primates is downward relative to the plane of the ventral border of the medulla (Fig. 4D,F,H,J). This differs from the plesiadapiforms *I. graybullianus* (Silcox et al., 2009), *M. annectens* (Silcox et al., 2010), and *P. tricuspidens* (not as downwardly orientated, Orliac et al., 2014). The downward shift of the olfactory bulbs (and reduction of their size) in Euprimates might be correlated with the orientation of the axis of the orbit and the reduction of the space for the brain left between the two orbits.

External morphology of the cerebrum

Neocortical sulci are variably present among Euprimates, and a great diversity of patterns is observed today. Eocene Euprimates also show different neocortical patterns, yet no complex pattern is documented to date (Fig. 4). The tarsiiforms *T. homunculus*, *R. viejaensis*, and *N. antiquus* are lissencephalic (Radinsky, 1970; Kirk et al., 2014), whereas a lateral sulcus is observed in the adapiforms *S. gracilis* (Gazin, 1965) and *A. parisiensis* (Radinsky, 1970; Gingerich and Martin, 1985), and here in the tarsiiform *M. erinaceus*. A lateral sulcus is also observed in the Plesiadapiforms *P. tricuspidens* and *Mi. annectens*. This suggests a complex evolutionary history of neocortical sulci pattern, with independent acquisition of the lateral sulcus. The lateral lobe in *M. erinaceus* and *Tarsius* presents a shallow sulcus. A similar shallow

sulcus is also observed in some modern Strepsirhines such as *Galago*, suggesting strong homoplasy for this character.

Ecological signal

Brain specialization can be seen in living primates according to certain ecological factors. For example, the size of the primary sensory structures has been linked to activity period in extant primates (Barton et al., 1995; Barton, 2001). Diurnal primates have larger visual cortices, whereas nocturnal primates generally show larger olfactory bulbs (Barton et al., 1995; Barton, 2001). Sensory brain structures have also been linked to diet in certain categories of primates; and diurnal frugivores will have larger visual cortices than folivores, as foraging for fruit relies heavily on vision (Clutton-Brock and Harvey, 1980; Barton, 1998, 2001). In nocturnal primates, frugivores have larger olfactory bulbs than folivores, as they rely more heavily on their sense of smell to forage for fruits (Barton et al., 1995; Barton, 1998). Dental microwear analysis performed on *Microchoerus* specimens from Perrière have revealed a diet based on fruit and gums (Ramdarshan et al., 2012), a similar diet to the coeval microchoerid *Necrolemur*. Both *Necrolemur* and *Microchoerus* also have a large procumbent incisor that shows signs of heavy wear (Schmid, 1983) indicative of scraping and gouging, confirming the microwear results obtained on the molars. Based on the size of the orbits, Kay and Kirk (2000) proposed that *Microchoerus* sp. had similar visual acuity to extant nocturnal primates.

Adapids and Microchoerids are found in the same localities in the late Eocene of Europe, suggesting these primates lived in similar environments and could have fed on the same resources. However, both groups developed different ecological strategies, limiting ecological overlap. Different activity cycles would imply different feeding times, and although both groups would have fed on fruits, other foods such as gums (microchoerids) or hard objects (adapids) would have implied a limited ecological overlap.

Optic nerve cross-section and orbit size. Interpretation of OFI and OFQ values for extinct taxa closely related to haplorhines is not straightforward. The OFI of *M. erinaceus* based on UM-PRR1771 falls both within the range of extant diurnal haplorhines and nocturnal strepsirrhines as illustrated by Silcox et al. (2010, see Supporting Information Fig. 3), whereas its OFQ falls between the values of nocturnal and diurnal haplorhines and in the largely overlapping ranges of extant strepsirrhines (see Supporting Information Fig. 3). Based on skull length and orbit diameter, UM-PRR1771 falls within the nocturnal strepsirrhine polygon of Kay and Kirk (2000: Fig. 8), but very close to the edge of the diurnal Haplorhines space. It also falls in the range of nocturnal strepsirrhines in the diagram of Ni et al. (2014: Fig. 4). In addition to the large diameter of its orbits, *M. erinaceus* also present a very shallow maxilla below the orbit (mid-facial depth) and the molar roots (M2) protrude in the orbital floor, a character related to eyeball hypertrophy (Seiffert et al., 2005), a condition observed in nocturnal primates (Kay and Kirk, 2000; Rosenberger, 2011). Coronal CT scan sections at the level of the distal root of M2 of UM-PRR1771 are provided in Supporting Information Figure 4.

Olfactory bulbs. In *M. erinaceus*, the olfactory bulbs occupy 0.96% of the overall braincase volume (Table 1). Among living primates, this value is more comparable to small bodied living haplorhine *Tarsius*, or to larger strepsirhines such as the lemurs *Avahi* and *Propithecus* (Stephan et al., 1981; Silcox et al., 2009). As illustrated on Figure 6B,C, *M. erinaceus* falls within the range of variation of Euprimates for the volume of the olfactory bulbs relative to body mass, and to endocranial volume. *M. erinaceus* and *N. antiquus* are closer to extant haplorhines than to extant strepsirhines for the olfactory bulb volume relative to body mass, while *T. homunculus* and *A. parisiensis* fit in the extant strepsirhines range (Fig. 6C).

Studies have shown than olfactory bulb size can be correlated to activity pattern in primates, with diurnal primates having smaller olfactory bulbs than nocturnal taxa. The latter rely more heavily on their sense of smell to forage for food, and less on visual clues (Barton, 1998). Based on its orbit size, *Microchoerus* sp. has been interpreted as nocturnal (Kay and Kirk, 2000), the same result is achieved here for *M. erinaceus*. By contrast, the latter shows smaller olfactory bulbs than its coeval *A. parisiensis*, a taxon which was most probably diurnal (Kay and Kirk, 2000). This would seem to contradict the pattern seen in extant primates. Barton (1998) suggested that olfactory bulb size was also correlated to other ecological factors such as habitat and diet. Indeed among strepsirhines, nocturnal frugivores have larger olfactory bulbs than folivores. However, *M. erinaceus* was a fruit and gum eater but shows olfactory bulbs more comparable in relative size to folivorous nocturnal/cathemeral strepsirhines such as *Propithecus*. Again, this seems to contrast with patterns observed in primates today.

Another important parameter is the evolutionary history of taxa and their phylogenetic position in the Euprimates tree. The size of the olfactory bulb carries a phylogenetic signal, which might also need to be taken into account, and reduction of the olfactory bulb volume could be synapomorphic of derived Tarsiiformes. On the other hand, the large olfactory bulbs seen in *A. parisiensis* could be related to the fact this taxon has a weakly flexed basicrania and relatively smaller orbits.

CONCLUSION

The endocranial cast of *Microchoerus erinaceus* documented by the virtual reconstruction of the endocranial cavity of UM-PRR1771 complements our knowledge of Tarsiiformes (or Omomyiformes, depending of the phylogenetic framework considered) in general, and of Microchoeridae in particular, so far only partly documented by *Necrolemur antiquus*. The gross morphology of the endocast of *M. erinaceus* shows the derived features observed in other Euprimates: demarcation of the temporal lobe, lack of exposure of the midbrain, a posterior location of the optic chiasma (closer to the pituitary), and presence of a sylvian fissure. *M. erinaceus* shows an already well encephalized brain, with large temporal lobes and limited but present folding consisting of a shallow lateral sulcus and an even shallower temporal sulcus. The latter is also observed in the extant haplorhine *Tarsius*. Together with an encephalized brain, *M. erinaceus* shows a telencephalic flexure comparable to that of extant strepsirhines and haplorhines such as *Cebuella* or *Hylobates*.

M. erinaceus is considered as nocturnal based on its orbits size, and had a diet based on fruit and gum.

However, its brain showed small olfactory bulbs, smaller than that of the diurnal coeval *Adapis parisiensis*. This observation also contrasts with patterns observed in primates today where nocturnal taxa have larger olfactory bulbs than diurnal taxa, and nocturnal frugivores have larger olfactory bulbs than folivores. *M. erinaceus* was a fruit and gum eater but shows olfactory bulbs more comparable in relative size to folivorous nocturnal/cathemeral strepsirhines such as *Propithecus*. Based on our results, the neocorticalization ratio of *M. erinaceus* is consistent with values calculated for other Late Eocene Euprimates including folivorous taxa, calling into question the direct correlation between frugivory and neocorticalization increase in primates.

Late Eocene primates already show a variety of brain morphologies, highlighting the complex history of the external features of the primate brain, as early as the Eocene. The brain of *M. erinaceus* is markedly different from that of its coeval *Adapis parisiensis*.

Various observations made here on the endocranial cast of Eocene Euprimates highlight the limits of use of correlations based on extant taxa, and that brain morphology results from complex variables, blending diverse ecological parameters, mechanical constraints, and phylogenetic heritage.

ACKNOWLEDGMENTS

The authors first want to acknowledge C. Zollikofer, of the Anthopological Institut and Museum, Zürich for access to CT scan facilities in Zürich. The authors are also grateful to R. Lebrun for his help with 3D data post-treatment, and to E. Gilissen, and L. Marivaux for fruitful comments on brain and primate evolution. The authors are grateful to L. Hautier, M. Low, and A. Heaver from the University of Cambridge for giving access to the Cambridge specimen of *Adapis parisiensis* and for performing the CT scan. The authors are grateful to M. Silcox and an anonymous reviewer for their constructive comments on early version of the manuscript. Data presented in this work were produced through the technical facilities of the MRI platform and of the labEx CeMEB. This is ISE-M Publication ISEM n° ISEM 2015-139.

LITERATURE CITED

Barton R. 2001. The evolutionary ecology of the primate brain. In: Lee PC, editor. Comparative primate socioecology. Cambridge: Cambridge University Press. p 167–203.

Barton R, Purvis A, Harvey PH. 1995. Evolutionary radiation of visual and olfactory brain systems in primates, bats and insectivores. Philos Trans R Soc Lond B 348:381–392.

Barton RA. 1998. Visual specialization and brain evolution in primates. Proc R Soc Lond B 265:1933–1937.

Biegert J. 1963. The evaluation of characteristics of the skull, hands and feet for primate taxonomy. In: Washburn SL, editor. Classification and human evolution. Chicago: Aldine. p 116–145.

Bloch JI, Silcox MT. 2006. Cranial anatomy of the Paleocene plesiadapiform *Carpolestes simpsoni* (Mammalia, Primates) using ultra high-resolution X-ray computed tomography, and the relationships of plesiadapiforms to Euprimates. J Hum Evol 50:1–35.

Bloch JI, Silcox MT, Boyer DM, Sargis EJ. 2007. New Paleocene skeletons and the relationship of plesiadapiforms to crown-clade primates. Proc Natl Acad Sci USA 104:1159–1164.

Clutton-Brock T, Harvey P. 1980. The evolutionary ecology of the primate brain. J Zool 190:309–325.

Conroy G. 1987. Problems of body-weight estimation in fossil primates. Int J Primatol 8:115–137.

Dagosto M, Terranova CJ. 1992. Estimating the body size of Eocene primates: a comparison of results from dental and postcranial variables. Int J Primatol 13:307–344.

Dechaseaux C. 1962. Cerveaux d'animaux disparus: essai de paléoneurologie, Vol. 24). Paris: Masson.

Diamond MK. 1992. Homology and evolution of the orbitotemporal venous sinuses of humans. Am J Phys Anthropol 88:211–244.

Dunbar RI, Shultz S. 2007. Evolution in the social brain. Science 317:1344–1347.

Eisenberg J. 1981. The mammalian radiations: an analysis of trends in evolution, adaptation, and behavior. Chicago: University of Chicago Press.

Ford SM, Davis LC. 1992. Systematics and body size: implications for feeding adaptations in New World monkeys. Am J Phys Anthropol 88:415–68.

Gazin C. 1965. An endocranial cast of the Bridger Middle Eocene primate, Smilodectes gracilis Smithsonian Miscellaneous Collection. Washington: Smithsonian Institution. p 1–14.

Gingerich PD, Smith BH, Rosenberg K. 1982. Allometric scaling in the dentition of primates and prediction of body weight from tooth size in fossils. Am J Phys Anthropol 58:81–100.

Gingerich P, Gunnell G. 2005. Brain of *Plesiadapis cookei* (Mammalia, Proprimates): surface morphology and encephalization compared with those of Primates and Dermoptera. Contrib Mus Paleontol 31:185–195.

Gingerich P, Martin R. 1981. Cranial Morphology and Adaptations in Eocene Adapidae. II. The Cambridge Skull of *Adapis parisiensis*. Am J Phys Anthropol 56:235–257.

Gregory W. 1915. I. On the relationship of the Eocene lemur *Notharctus* to the Adapidæ and to other primates: II. On the classification and phylogeny of the Lemuroidea. Geol Soc Am Bul 26:419–446.

Gurche JA. 1982. Early primate brain evolution. In: Armstrong E, Falk D, editors. Primate brain evolution. New York, Plenum Press. p 227–246.

Hürzeler J. 1948. Zur Stammesgeschichte der Necrolemuriden. Basel: VerlagBirkhäuser.

Jerison H. 1973. Evolution of the Brain and Intelligence. New York: Academic Press.

Jerison HJ. 2012. Digitized fossil brains: neocorticalization. Biolinguistics 6:383–392.

Kay RF, Kirk EC. 2000. Osteological evidence for the evolution of activity pattern and visual acuity in primates. Am J Phys Anthropol 113:235–262.

Kirk EC, Daghighi P, Macrini TE, Bhullar BAS, Rowe TB. 2014. Cranial anatomy of the Duchesnean primate *Rooneyia viejaensis*: new insights from high resolution computed tomography. J Hum Evol 74:82–95.

Kirk E, Kay R. 2004. The evolution of high visual acuity in the Anthropoidea. In: Ross CF, Kay RF, editors. Anthropoid origins. New York: Springer US. p 539–602.

LaBarbera M. 2007. Analyzing body size as a factor in ecology and evolution. Annu Rev Ecol Syst 20:97–117.

Lebrun R. 2014. ISE-MeshTools, a 3D interactive fossil reconstruction freeware. 12th Annual Meeting of EAVP, Torino, Italy.

Long A, Bloch JI, Silcox MT. 2015. Quantification of neocortical ratios in stem primates. Am J Phys Anthropol 157:363–373.

Martin R. 1990. Primate origins and evolution: a phylogenetic reconstruction. Princeton: Princeton University Press.

McCarthy RC. 2001. Anthropoid cranial base architecture and scaling relationships. J Hum Evol 40:41–66.

Meng J, Hu Y, Li C. 2003. Theosteology of *Rhombomylys* (Mammalia, Glires): implications for phylogeny and evolution of Glires. Bul Am Mus Nat Hist 275:1–247.

Ni X, Gebo DL, Dagosto M, Meng J, Tafforeau P, Flynn JJ, Beard KC. 2013. The oldest known primate skeleton and early haplorhine evolution. Nature 498:60–64.

Orliac MJ, Ladevèze S, Gingerich PD, Lebrun R, Smith T, Ladeve S. 2014. Endocranial morphology of Palaeocene *Plesiadapis tricuspidens* and evolution of the early primate brain. Proc R Soc Lond B 281:2013-2792.

R Core Team. 2015. R: A language and environment for statistical computing. Vienna, Austria: R Foundation for Statistical Computing. Available at: http://www.R-project.org/.

Radinsky L. 1967. The oldest primate endocast. Am J Phys Anthropol 27:385–388.
Radinsky L. 1968. A new approach to mammalian cranial analysis, illustrated by examples of prosimian primates. J Morphol 124:167–180.
Radinsky L. 1970. The fossil evidence of prosimian brain evolution. In: Noback C, Montagna W, editors. The primate brain. Advances in primatology, Vol. 1. New York: Appleton-Century-Crofts. p 209–224.
Radinsky L. 1974. Prosimian brain morphology: functional and phylogenetic implications. In: Martin R, Doyle G, Walker A, editors. Prosimian biology. London: Duckworth. p 781–798.
Ramdarshan A, Marivaux L, Merceron G. 2011. Dental microwear texture analysis of three large bodied adapids from the late Eocene of the Quercy fissure fillings. In: Lehmann T, Schaal SFK, editors. The world at the time of Messel: Puzzles in palaeobiology, palaeoenvironment and the history of Early Primates. 22nd International Senckenberg Conference, November 1-5, Frankfurt, Am Main. pp 137–138.
Ramdarshan A, Merceron G, Marivaux L. 2012. Spatial and temporal ecological diversity amongst Eocene primates of France: evidence from teeth. Am J Phys Anthropol 147:201–216.
Rosenberger A, Hogg R, Wong S. 2008. *Rooneyia*, postorbital closure, and the beginnings of the age of Anthropoidea. In: Sargis EJ, Dagosto M, editors. Mammalian Evolutionary Morphology- A Tribute to Frederick S. Szalay. New York: Springer. p. 325–346.
Rosenberger AL. 2006. Protoanthropoidea (Primates, Simiiformes): A New Primate Higher Taxon and a Solution to the *Rooneyia* Problem. J Mamm E 13:139–146.
Ross CF, Ravosa MJ. 1993. Basicranial flexion, relative brain size, and facial kyphosis in nonhuman primates. Am J Phys Anthropol 91:305–324.
Ross C, Henneberg M. 1995. Basicranial flexion, relative brain size, and facial kyphosis in Homo sapiens and some fossil hominids. Am J Phys Anthropol 98:575–593.
Rowe TB, Macrini TE, Luo Z-X. 2011. Fossil evidence on origin of the mammalian brain. Science 332:955–957.
Schmid P. 1983. Front dentition of the omomyiformes (primates). Folia Primatol 40:1–10.
Seiffert ER, Simons EL, Clyde WC, Rossie JB, Attia Y, Bown TM, Chatrath P, Mathison ME. 2005. Basal anthropoids from Egypt and the antiquity of Africa's higher primate radiation. Science 310:300–304.
Sigé B, Jaeger J-J, Sudre J, Vianey-Liaud M. 1990. Altiatlasius koulchii n. gen. et sp., primate omomyidé du Paléocène supérieur du Maroc, et les origines des euprimates. Palaeontogr Abt A A:31–56.
Silcox MT, Benham AE, Bloch JI. 2010. Endocasts of *Microsyops* (Microsyopidae, Primates) and the evolution of the brain in primitive primates. J Hum Evol 58:505–521.
Silcox MT, Dalmyn CK, Bloch JI. 2009. Virtual endocast of *Ignacius graybullianus* (Paromomyidae, Primates) and brain evolution in early primates. Proc Nat Acad Sci USA 106: 10987–10992.
Simons E, Russell D. 1960. Notes on the cranial anatomy of *Necrolemur*. Breviora 127:1–14.
Smith RJ. 2002. Estimation of body mass in paleontology. J Hum Evol 43:271–287.
Spoor F. 1997. Basicranial architecture and relative brain size of Sts 5 (*Australopithecus africanus*) and other Plio-Pleistocene hominids. S Afr J Sci 93:182–186.
Stephan H. 1984. Morphology of the brain in *Tarsius*. In: Niemetz C, editor. Biology of tarsiers. Stuttgart: Gustav Fischer Verlag. p 319–344.
Stephan H, Frahm H, Baron G. 1981. New and revised data on volumes of brain structures in insectivores and primates. Folia Primatol 35:1–29.
Szalay FS. 1976. Systematics of the Omomyidae (Tarsiiformes, Primates): taxonomy, phylogeny, and adaptations. Bul Am Mus Nat Hist 156:159–449.